Sensor and Simulation Notes

Note 548

October 2009

Design of a rectangular waveguide narrow-wall longitudinal-aperture array using microwave network analysis

Naga R. Devarapalli, Carl E. Baum, Christos G. Christodoulou, Edl Schamiloglu

University of New Mexico, Albuquerque, NM 87131, USA

ABSTRACT

A rectangular waveguide narrow-wall longitudinal-aperture array (slot array) is designed to perform as close to a uniform array with minimum power reflected into the feed-waveguide as possible using microwave network analysis. The array is designed by optimizing the mutual coupling through the waveguide between the elements. For this analysis, the external coupling between the array elements is ignored.

The mutual coupling analysis is performed using microwave theory. The first four elements of the array are reduced to lossy two-port networks. The last element of the array, called the H-plane-bend-radiator [1], is reduced to a lossy one-port network. The loss in a network represents the power radiated by the corresponding element. The S-parameters and the phases of the array elements are obtained from computational analysis performed using HFSS (High Frequency Structure Simulator). This discussion is presented in detail in [1]. The phase of an element is the phase of the aperture E-field at the center of the aperture and is measured relative to the phase of the input power, which is equal to zero at the input port of the array.

I. INTRODUCTION

It is assumed that the slot array's feed-waveguide only supports the TE_{10} mode, the dominant mode in a rectangular waveguide. The slot array shown in Fig. 1(a) consists of longitudinal-slots in the narrow wall of a rectangular waveguide; the behavior of these slots is presented in [1]. The center-to-center distance between any two adjacent array elements is the same.

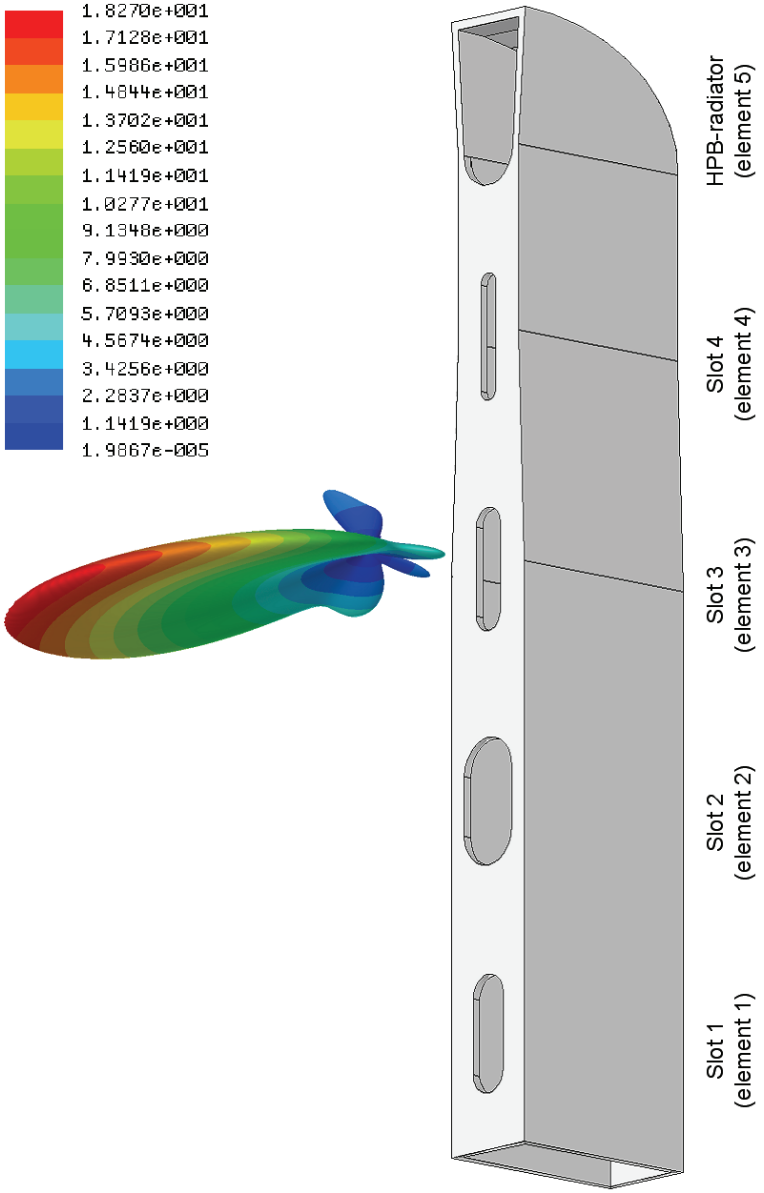

Fig. 1(a). Slot array along with its 3-D radiation power pattern in absolute units.
Note that all of the input energy at the feed-waveguide is assumed to be in the dominant mode.

The idea for the array is based on the work presented in [2]. The array radiates a fan beam pattern and its radiated electric (E-) fields are strongly linearly polarized in the direction of the broad dimension of the fan-beam pattern. The slot array shown in Fig. 1(a) is a complementary structure to the one shown in Fig. 1(b), which is described in [3]. Both structures produce a fan beam radiation pattern with the radiated E-field polarization of one structure orthogonal to that of the other.

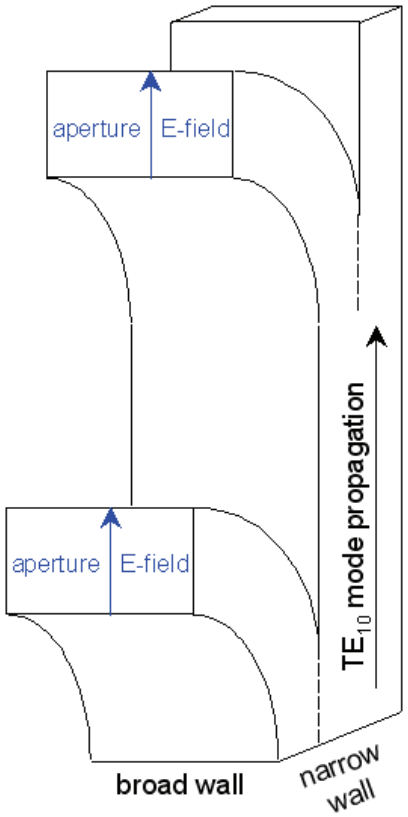

Fig. 1(b). Complementary structure to the slot array.

The design criteria for the slot array are to maximize the peak directivity of its fan-beam radiation pattern and to minimize the reflected power into its feed-waveguide. The design variables are the dimensions of the slots, spacing between the elements and the narrow-wall taper. The narrow wall of the waveguide can be squeezed at a certain location along the length of the guide to increase the power radiated by a specific slot.

To maximize the peak directivity of the array, the elements of the array are to radiate equal powers and have a progressive phase shift, i.e. the design is to produce a uniform linear array. To minimize the power reflected into the feed-waveguide, the powers reflected from the individual elements need to destructively interfere. The optimal array design is a best compromise between the powers radiated by the elements, the progressive phase shift between the elements and the reflected power at the input of the array. Note that the analysis presented is in the X-band, at 10GHz.

The H-plane-bend-radiator (HPB-radiator) is an H-plane bend terminating in a radiating aperture with the narrow dimension of the waveguide flaring out; its design is described in [1]. The HPB-radiator shown in Fig. 1(a) produces very low reflected power at its input and has a radiation pattern that is consistent with the element pattern of the slot array.

II. MICROWAVE NETWORK ANALYSIS

Figure 2 shows the slot array in Fig. 1(a) represented as a microwave network. P_{in1} through P_{in5} are the powers being input at the input ports of array elements 1 through 5 respectively. P_{rad1} through P_{rad5} are the powers radiated by array elements 1 through 5 respectively. Γ_1 through Γ_5 are the reflection coefficients under matched port conditions. For instance, Γ_1 is affected by the presence of slot 1 through slot 4 and the HPB-radiator and is the effective reflection coefficient at the input of the network shown, but assumes that the input of the network is a matched port.

Γ_2 through Γ_5 in Fig. 2 contribute to mutual coupling between the array elements and in the ideal case scenario it is better to have Γ_1 through Γ_5 equal to zero. In addition to the obvious reason for the reflected power to be minimized so as to maximize antenna efficiency/gain and

protect the high power microwave source, an additional reason is as follows. There is a good possibility that the radiation pattern of the array would have its main lobe canted from the broadside direction, and since the design goal is to maximize the directivity, it is advantageous to have power flow in only one direction along the length of the linear array.

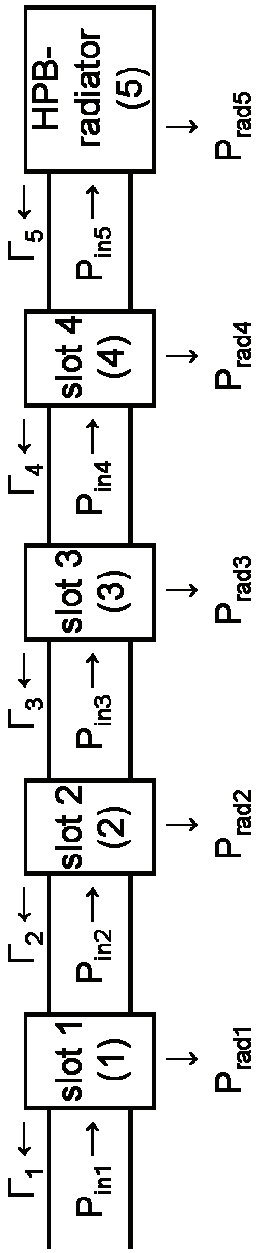

Fig. 2. Equivalent microwave network of the slot array.

Although the powers radiated by all the elements (represented by P_{rad}s in Fig. 2) need to be equal, the fraction of the power radiated to the amount of power being input to a certain

element is different from the other elements. For instance, in the ideal case scenario: when Γ_1 through Γ_5 are equal to zero, the optimal values for P_{rad1} through P_{rad5} are given by $0.2P_{in1}$, $0.25P_{in2}$, $P_{in3}/3$, $0.5P_{in4}$, P_{in5} respectively. Since, in reality Γ_1 through Γ_5 are not equal to zero, the goal of the microwave network analysis is to obtain expressions for Γ_1, P_{rad1} through P_{rad5} in terms of: P_{in1}, the S-parameters of the array elements 1 through 5, and the distance between the array elements. The effect of mutual coupling on: the aperture phases obtained from computational analysis of the array elements 1 through 5, is factored in by simply knowing the distance between the elements and the phase of the input powers P_{in1} through P_{in5}. Hence, the aperture phase of slot 1 is only influenced by the phase of P_{in1} and the location of the array's input port from slot 1. Similarly, the aperture phase of slot 2 is only influenced by the phase of P_{in2} and the distance between slot 1 and slot 2. This aperture phase calculation procedure can be similarly extended to the array elements 3 through 5. Note that the aperture phase calculations assume that the Γ s are small enough and therefore do not influence them.

The expressions for Γ_1, P_{rad1} through P_{rad5}, and the aperture phases are then implemented in an iterative program whose inputs are the S-parameters and aperture phases for narrow-wall longitudinal-slots of various dimensions obtained from computational analysis in HFSS. The program iterates on the possible distances/dimensions between/of the array elements without exceeding the maximum length constraint on the array, to find the best combination of slots' dimensions and inter-element spacing that produces the optimal slot array design.

The microwave network analysis is started by beginning at the HPB-radiator element and progressing towards the array input, one element at a time, until slot 1 is reached ('reverse-path analysis'); then by progressing from slot 1 towards the end of the array, one element at a time, until the HPB-radiator element is reached ('forward-path analysis'), completes the analysis. The

goal of the reverse (forward) path analysis is to obtain the expression(s) for Γ_1 (P_{rad1} through P_{rad5}) in terms of P_{in1}, the S-parameters of the array elements 1 through 5, and the distance between the array elements.

The inter-element spacing between the array elements can be embedded as a phase shift in the S-parameters of the individual elements. This can be achieved by 'a shift in reference planes', and is discussed in detail in the section on 'the scattering matrix' in [4].

II.a. REVERSE-PATH ANALYSIS

The first step in the reverse-path analysis is illustrated in Fig. 3. 'Load 5' in Fig. 3 represents the array element 5. V_1^+, V_2^+, V_1^-, V_2^- in Fig. 3 represent the voltage waves that are well known in the microwave network analysis performed using S-parameters. Following standard S-parameter network analysis, the network shown in Fig. 3 satisfies Eqs. 1, 2 and 3; S_{11}, S_{12}, S_{21}, S_{22} represent the S-parameters of the two-port network that represents slot 4; Γ_5 is the reflection coefficient of the one-port network (load 5) that represents the HPB-radiator under matched port condition.

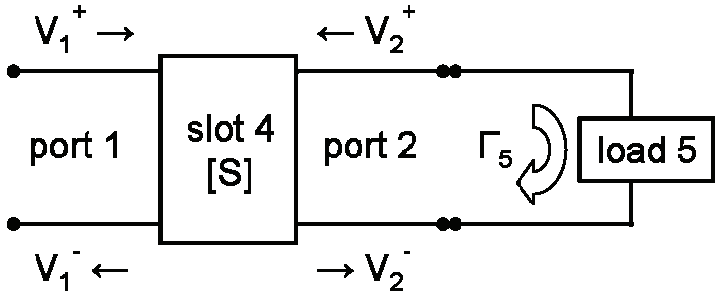

Fig. 3. Illustration for the first step in the reverse-path analysis.

$$V_2^+ = \Gamma_5 V_2^- \qquad \textbf{(1)}$$

$$V_2^- = S_{21} V_1^+ + S_{22} V_2^+ \qquad \textbf{(2)}$$

$$V_1^- = S_{11} V_1^+ + S_{12} V_2^+ \qquad \textbf{(3)}$$

Equations 1, 2 and 3 can be solved to obtain the expressions in Eqs. 4 through 10. The reflection coefficient when port 1 of the network in Fig. 3 is matched, Γ_4, shown in Eq. 6 is calculated and recorded to be used in the second step of the reverse-path analysis.

$$\frac{V_2^-}{V_1^+} = \frac{S_{21}}{1-\Gamma_5 S_{22}} \quad \textbf{(4)}$$

$$\frac{V_2^+}{V_1^+} = \frac{\Gamma_5 S_{21}}{1-\Gamma_5 S_{22}} \quad \textbf{(5)}$$

$$\Gamma_4 = \frac{V_1^-}{V_1^+} = S_{11} + \Gamma_5 S_{12}\frac{V_2^-}{V_1^+} \quad \textbf{(6)}$$

$$P_{in5} = P_{in4}\left|\frac{V_2^-}{V_1^+}\right|^2 \quad \textbf{(7)}$$

$$P_{ref\,4} = P_{in4}\left|\Gamma_4\right|^2 \quad \textbf{(8)}$$

$$P_{load5} = P_{in4}\left(\left|\frac{V_2^-}{V_1^+}\right|^2 - \left|\frac{V_2^+}{V_1^+}\right|^2\right) \quad \textbf{(9)}$$

$$P_{rad4} = P_{in4} - P_{ref\,4} - P_{load5} \quad \textbf{(10)}$$

where:

P_{in4} is the power being input at port 1 of the two-port network that represents slot 4 in Fig. 3

P_{ref4} is the power reflected at port 1 in Fig. 3 under matched port conditions

P_{load5} is the power delivered to the HPB-radiator

P_{rad4} is the power radiated by slot 4

In the second step of the reverse-path analysis, the complete network in Fig. 3 is considered as a single one-port network (labeled as 'load 4' in Fig. 4) with Γ_4 computed in Eq. 6

representing its reflection coefficient under matched port condition. This one-port network is now connected to the equivalent two-port network for slot 3 as shown in Fig. 4. From this point, the analysis of this two-port network connected to the one-port network continues in the same way as in step one of the reverse-path analysis. The reflection coefficient at port 1 in Fig. 4 (Γ_3) is obtained. In addition, the following expressions are obtained in terms of the power being input at port 1 of the two-port network that represents slot 3 in Fig. 4 (P_{in3}): the power reflected at port 1 in Fig. 4 (P_{ref3}), the power delivered to load 4 (P_{load4}) and the power radiated by slot 3 (P_{rad3}).

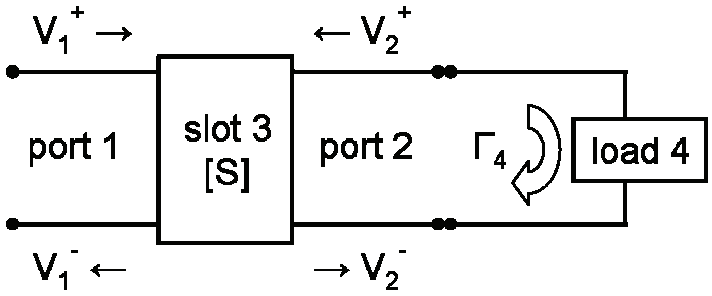

Fig. 4. Illustration for the second step in the reverse-path analysis.

The reverse-path analysis procedure is complete when it is carried out all the way until the first element (i.e. slot 1), at which point the value of the effective reflection coefficient at the input of the complete network as shown in Fig. 2 (Γ_1) is found. Note that P_{rad1} through P_{rad5} cannot be computed in the reverse-path analysis, since P_{in1} through P_{in5} are unknown.

II.b. FORWARD-PATH ANALYSIS

The forward-path analysis also has a series of steps similar to the reverse-path analysis, and the first step is illustrated in Fig. 5. 'Load 2' in Fig. 5 includes array elements 2 through 5. It can be inferred that by starting from a known value for P_{in1}, the values for P_{rad1} and P_{in2} can be found from the first step of the forward-path analysis. The second step of the forward-path analysis is illustrated in Fig. 6. 'Load 3' in Fig. 6 includes array elements 3 through 5. From the value of P_{in2} obtained from the first step of the forward-path analysis, the values for P_{rad2} and

P_{in3} are found from the second step of the forward-path analysis. This analysis is complete when it is continued to eventually find all the powers radiated by the array elements, P_{rad1} through P_{rad5}.

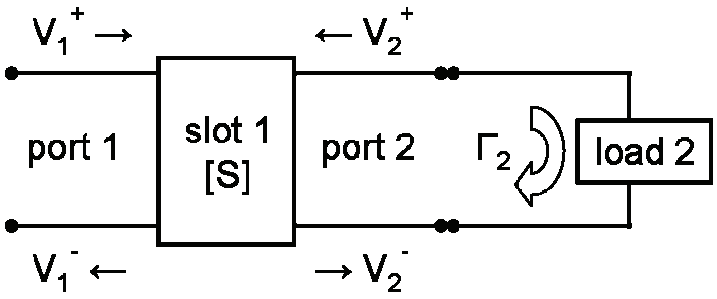

Fig. 5. Illustration for the first step in the forward-path analysis.

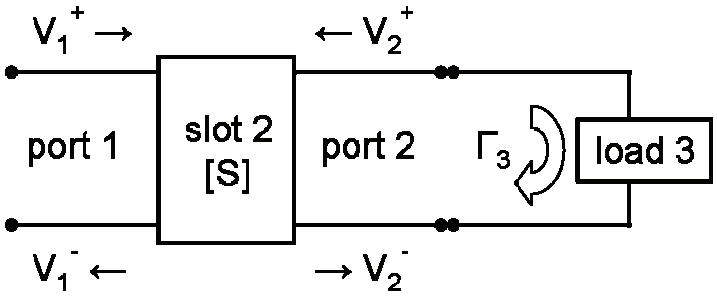

Fig. 6. Illustration for the second step in the forward-path analysis.

II.c. IMPLEMENTATION OF THE MICROWAVE NETWORK ANALYSIS

The S-parameters and aperture phases of the individual array elements are obtained from HFSS simulations and the coupling analysis is implemented in a routine that iterates on the dimensions of the slots and the distance between the array elements. The routine was coded in MATLAB (Matrix Laboratory).

It is not possible to achieve the ideal case scenario: i.e. when Γ_1 through Γ_5 are equal to zero, the optimal values for P_{rad1} through P_{rad5} are given by $0.2P_{in1}$, $0.25P_{in2}$, $P_{in3}/3$, $0.5P_{in4}$, P_{in5} respectively. Hence the MATLAB routine was run for the following optimization criteria. The mean offset between the radiated powers was minimized with the following additional criteria imposed: the reflected power at the array input < 5% of the input power, the mean error in the

progressive phase shift < 5°. The inputs to the routine were the S-parameters and aperture phases of slots with lengths (widths) varying between 14mm (0.5mm) and 15mm (8mm), and the S-parameter and aperture phase of the optimal HPB-radiator element for the slot array (presented in [1]). Note that 15mm corresponds to a half free-space wavelength at 10GHz.

The optimal values obtained from the MATLAB routine for the reflected power, mean error in the progressive phase shift, mean offset between the radiated powers are: <1% of the input power, 4.7°, 1.2% respectively. The optimal spacing between the slots that achieved these results was $11\lambda_g/16$, where λ_g is the guide wavelength for an X-band waveguide operating at 10GHz. Also, there is a narrow-wall flare introduced near the array element 4, as shown in Fig. 1, where the narrow dimension of the waveguide is squeezed by 20% to increase the radiated power through slot 4.

Table 1 shows the optimal dimensions for slot 1 through slot 4, along with the powers radiated and aperture phases of the array elements 1 through 5. The aperture phase is the phase of the aperture E-field at the center of the aperture with reference to the phase of the input power (=0°) at the input port of the array.

Array element	Slot dimensions	Radiated power	Aperture phase	Phase shift (mean=93.7°)
slot 1	14 x 5mm	19.8%	194.4°	93.3°
slot 2	15 x 8mm	19.6%	287.7°	94.4°
slot 3	14.5 x 4mm	19.8%	22.1°	84.6°
slot 4	15 x 2.5mm	17.5%	106.7°	102.3°
HPB-radiator		22.9%	209°	

Table 1. Results from mutual coupling optimization between the array elements. The radiated power is given as a percentage of the input power to the array. The aperture phase is the phase of the aperture E-field at the center of the aperture with reference to the phase of the input power (=0°) at the input port of the array.

III. FULL-WAVE ANALYSIS

Since the results in Table 1 do not include any external coupling between the array elements, the array is also simulated in HFSS using the optimal dimensions for the slots obtained from the MATLAB routine; the results from the HFSS simulation are as follows. The reflected power at the input of the array is <1% of the input power. Table 2 compares the values for the powers radiated and aperture phases of the array elements 1 through 5 obtained from this full-wave analysis with the optimized result from the MATLAB routine that uses microwave network analysis. Table 2 shows that there is good agreement between the microwave network analysis result and the full-wave analysis result.

	Microwave network analysis		Full-wave analysis	
Array element	Power radiated	Aperture phase	Power radiated	Aperture phase
slot 1	19.8%	194.4°	20.5%	202.3°
slot 2	19.6%	287.7°	20.4%	290.4°
slot 3	19.8%	22.1°	20.1%	31.7°
slot 4	17.5%	106.7°	16.8%	109.1°
HPB-radiator	22.9%	209°	22%	207.6°

Table 2. Results from microwave network analysis and full-wave analysis. The power radiated is given as a percentage of the input power to the array. The aperture phase is the phase of the aperture E-field at the center of the aperture with reference to the phase of the input power (=0°) at the input port of the array.

IV. DOUBLE ARRAY

The peak gain for the optimized slot array is approximately 12.6dB; this gain can be increased to approximately 14.9dB when the array configuration shown in Fig. 7 is used. The double array, shown in Fig. 7, is obtained from two slot arrays as follows. The double array consists of two identical slot arrays with a common broad wall; the slots are moved as close to

the common wall as possible. In the double array configuration, the apertures of one slot array alternate with those of the other slot array and the center-to-center distances between the elements of the double array are equal. The input phase of one array also needs to be appropriately phase shifted from the other, such that the aperture phases of the elements of the double array are in approximately a constant phase progression.

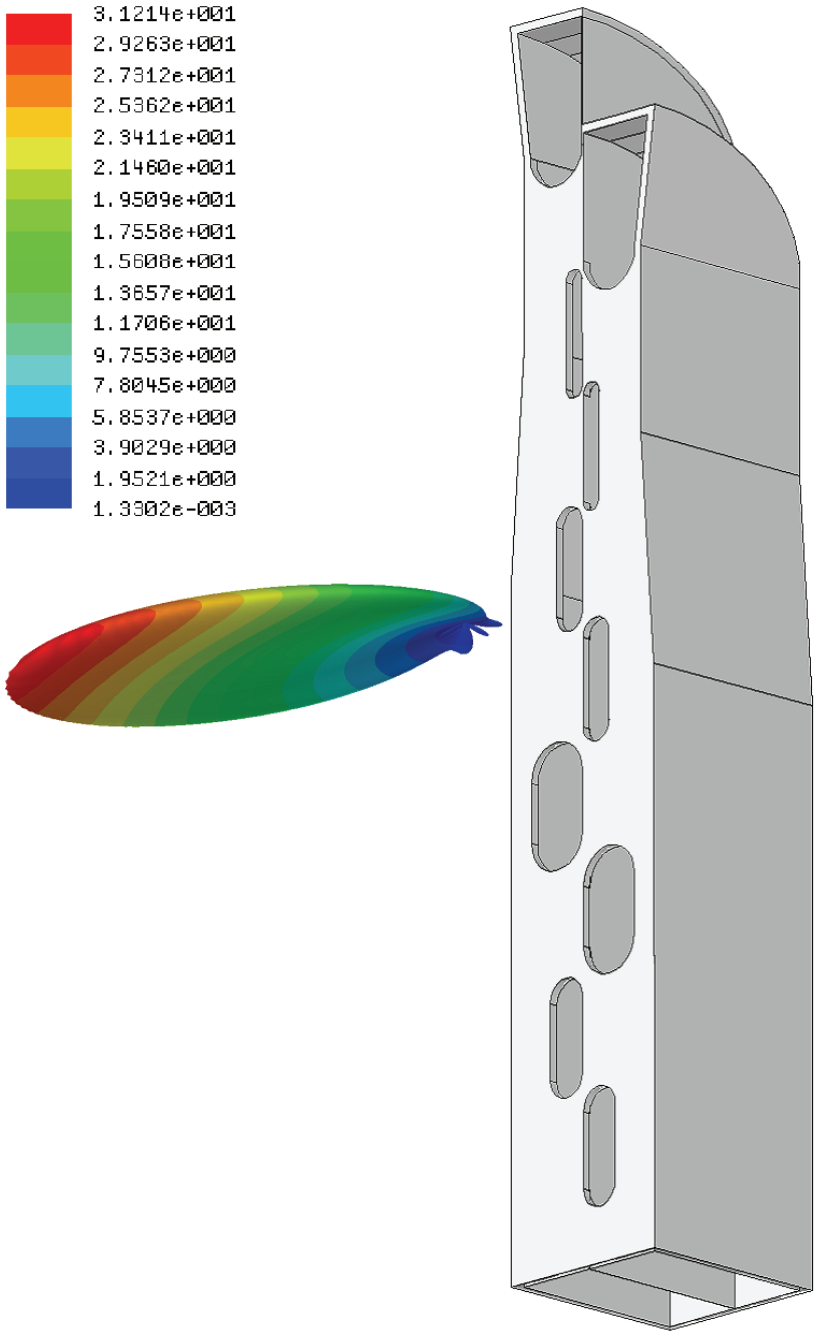

Fig. 7. Double array along with its 3-D radiation power pattern in absolute units.

The double array has essentially the same overall length as the slot array, but by increasing the number of elements in the array that are in approximately a constant favorable phase progression, a higher gain is achieved. In other words, the aperture field distribution of the double array is more uniform than that of the slot array, thereby resulting in a higher gain for the double array.

The aperture phases/magnitudes of an antenna array interfere constructively or destructively in various directions to produce the 3-D radiation pattern. For a pencil-beam-antenna-array that radiates a perfect pencil-beam radiation pattern, its aperture phases/magnitudes are such that they constructively interfere in a very narrow set of adjacent angles in approximately the same direction that the element pattern's maxima is directed, and in the rest of the angles the aperture phases/magnitudes of the array interfere destructively.

The double array produces a radiation pattern that is more similar to the pencil-beam-antenna-array's radiation pattern, when compared to the slot array. Figure 8 shows that the higher gain of the double array compared to that of the slot array is achieved by suppressing the side lobes. Note that the vertical axis in Figs. 8 and 9 represents the 'normalized' power radiated.

Figure 8 compares the H-plane radiation power patterns of the slot array and the double array; $\theta = 0^{o}$ on the horizontal axis of the plot in Fig. 8 corresponds to the broadside direction. The H-plane radiation power pattern of the double array was shifted by 1^{o}, so that the peaks of both patterns line up for making the beam-width comparison easier.

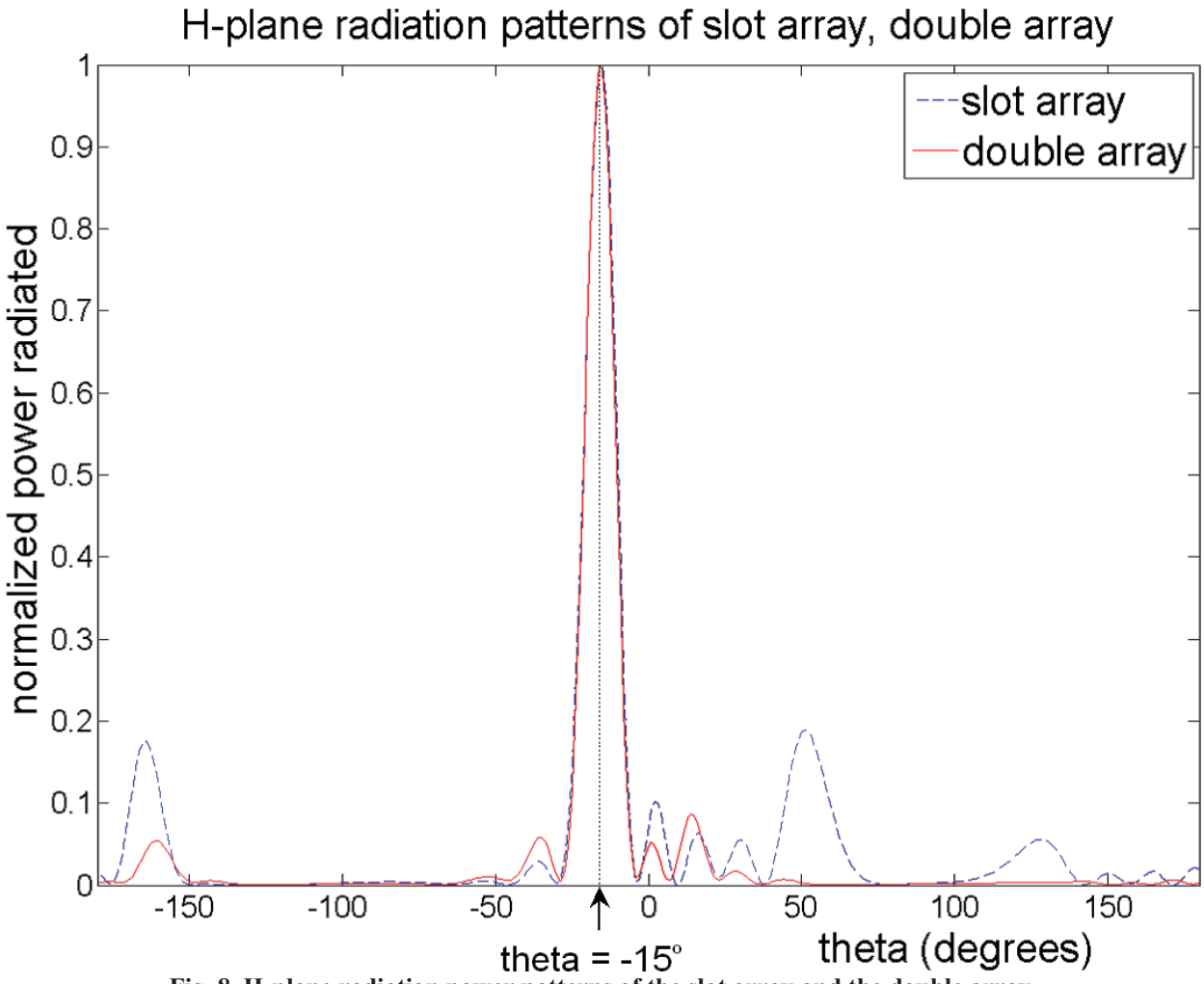

Fig. 8. H-plane radiation power patterns of the slot array and the double array.

Figure 9 compares the radiation power patterns of the slot array and the double array in the plane cut that is orthogonal to the H-plane and passing through the $\theta = -15^{o}$ line shown in Fig. 8; $\theta = 0^{o}$ on the horizontal axis of the plot in Fig. 9 corresponds to the same spatial point in the 3-D radiation power pattern as $\theta = -15^{o}$ on the horizontal axis of the plot in Fig. 8.

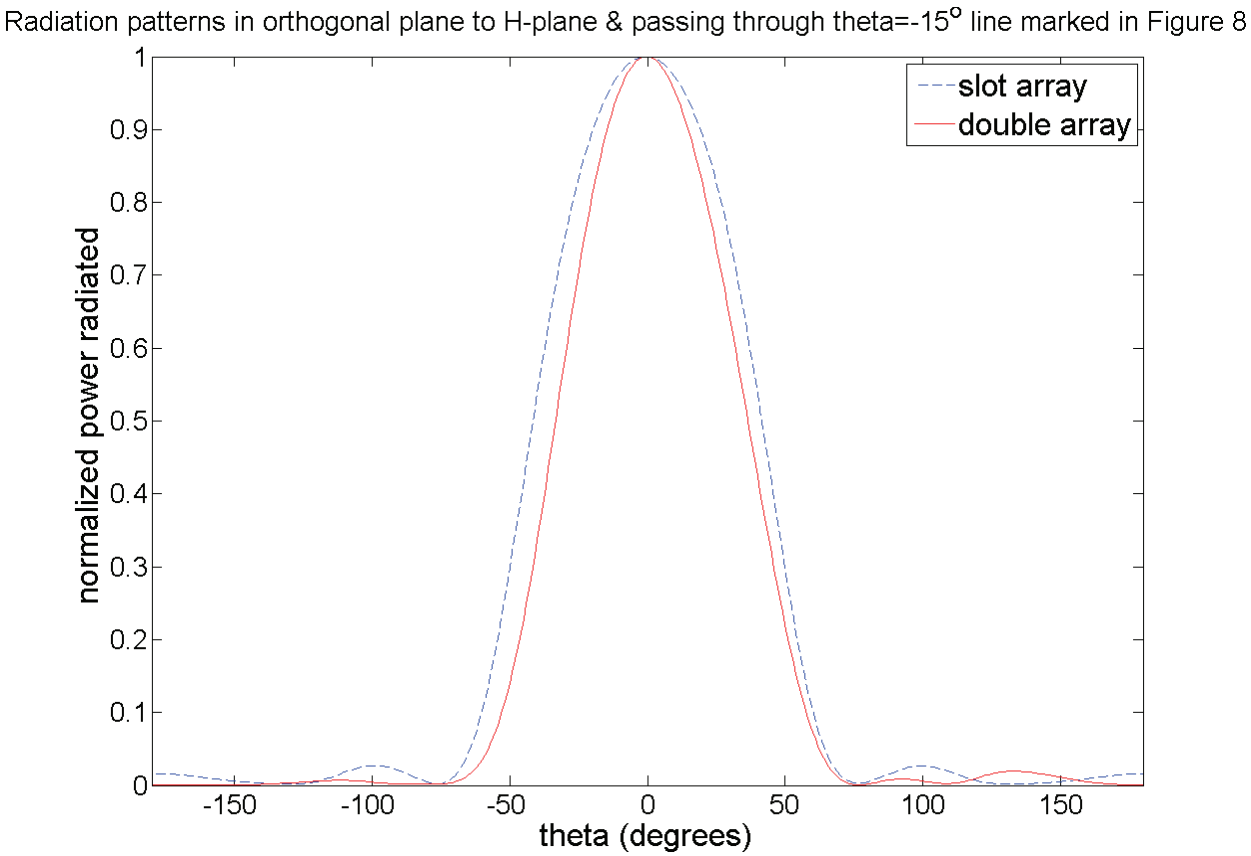

Fig. 9. Radiation power patterns of the slot array and the double array in the plane cut orthogonal to the H-plane and passing through the θ = -15° line shown in Fig. 8.

V. EXPERIMENTAL RESULTS

The analysis presented so far relies on the accuracy of the HFSS results. The objective of this section is to test the strength of an HFSS result, by comparing it to the corresponding experimental result. The experiment was conducted in the X-band, at 10GHz. The feed-guide is therefore a standard WR-90 waveguide. Figure 10 shows the structure of the slot array used for the experimental verification.

Theoretically, the narrow-wall flare in a rectangular waveguide only affects the power density inside the guide and has no effect on the propagating dominant mode structure, as long as the maximum dimension achieved by the narrow wall of the waveguide still only supports the dominant (TE_{10}) mode and not any higher order modes. Therefore the narrow-wall flare should

not dominate the skewing of the experimental results from theory. Removing the narrow-wall flare for experimental verification purposes is very desirable since it greatly reduces the machining complexity.

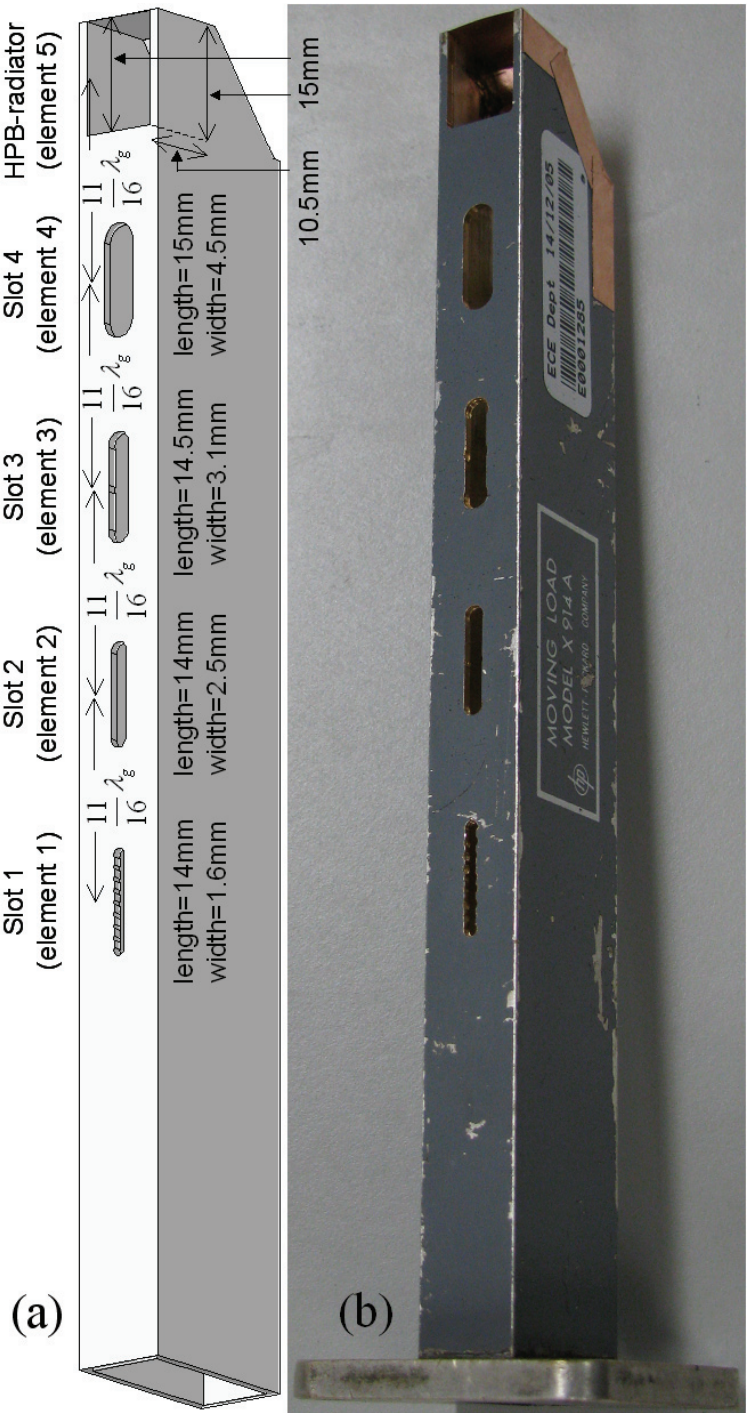

Fig. 10. (a) Schematic of the X-band slot array for experimental verification. λ_g is the guide wavelength for an X-band/WR-90 waveguide operating at 10GHz. (b) X-band slot array used for experimental verification.

A slot-array's design without any narrow-wall flare is verified with the same structure's simulation results. A schematic of the X-band slot array used to generate the full-wave analysis results in HFSS is shown in Fig. 10(a). Figure 10(b) shows the actual X-band slot array used for obtaining the experimental results. Figure 10(a) shows the dimensions of the array elements 1 through 5 and the inter-element spacing used in the X-band slot array's design for experimental verification.

The reflection coefficient, E and H-plane radiation patterns of the slot array that are obtained from HFSS are verified experimentally. The slotted line technique [4] is used to measure the reflection coefficient at the input of the slot array shown in Fig. 10. The theoretical, experimental values of the reflection coefficient are $0.17\angle 162°$, $0.18\angle 155°$ respectively. The theoretical, experimental radiation patterns are compared in Figs. 11, 12. There is good agreement between the theoretical and experimental results.

Figure 11 compares the theoretical and experimental H-plane radiation power patterns of the X-band slot array design; $\theta = 0^o$ on the horizontal axis of the plot in Fig. 11 corresponds to the broadside direction of the X-band slot array. The experimental H-plane radiation power pattern is shifted by 4^o in Fig. 11, so that the peaks of both patterns line up for making beam-width comparison easier.

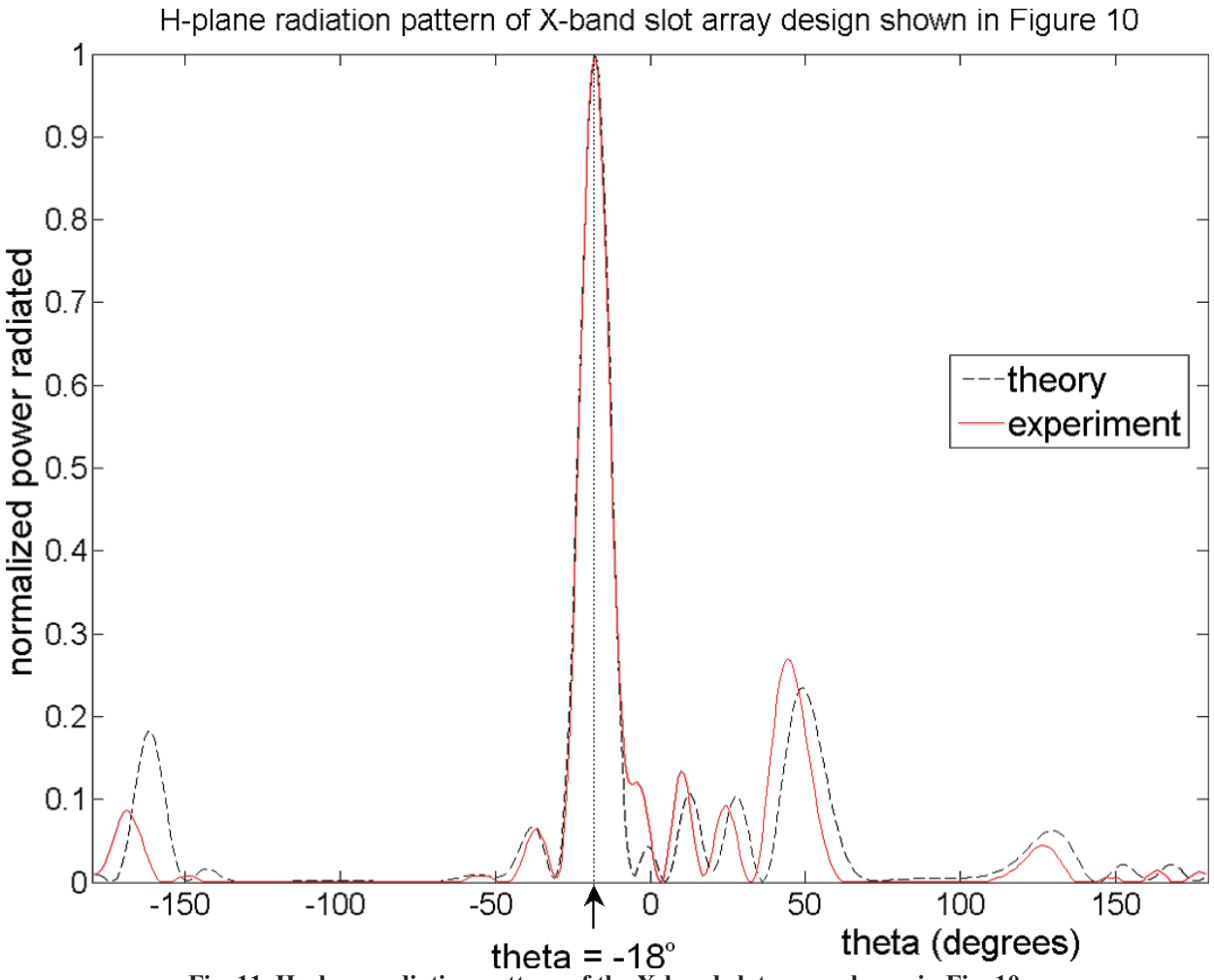

Fig. 11. H-plane radiation pattern of the X-band slot array shown in Fig. 10.

Figure 12 compares the theoretical and experimental radiation power patterns of the X-band slot array design in the plane cut that is orthogonal to the H-plane and passing through the $\theta = -18^{o}$ line shown in Fig. 11; $\theta = 0^{o}$ on the horizontal axis of the plot in Fig. 12 corresponds to the same spatial point in the 3-D radiation power pattern as $\theta = -18^{o}$ on the horizontal axis of the plot in Fig. 11.

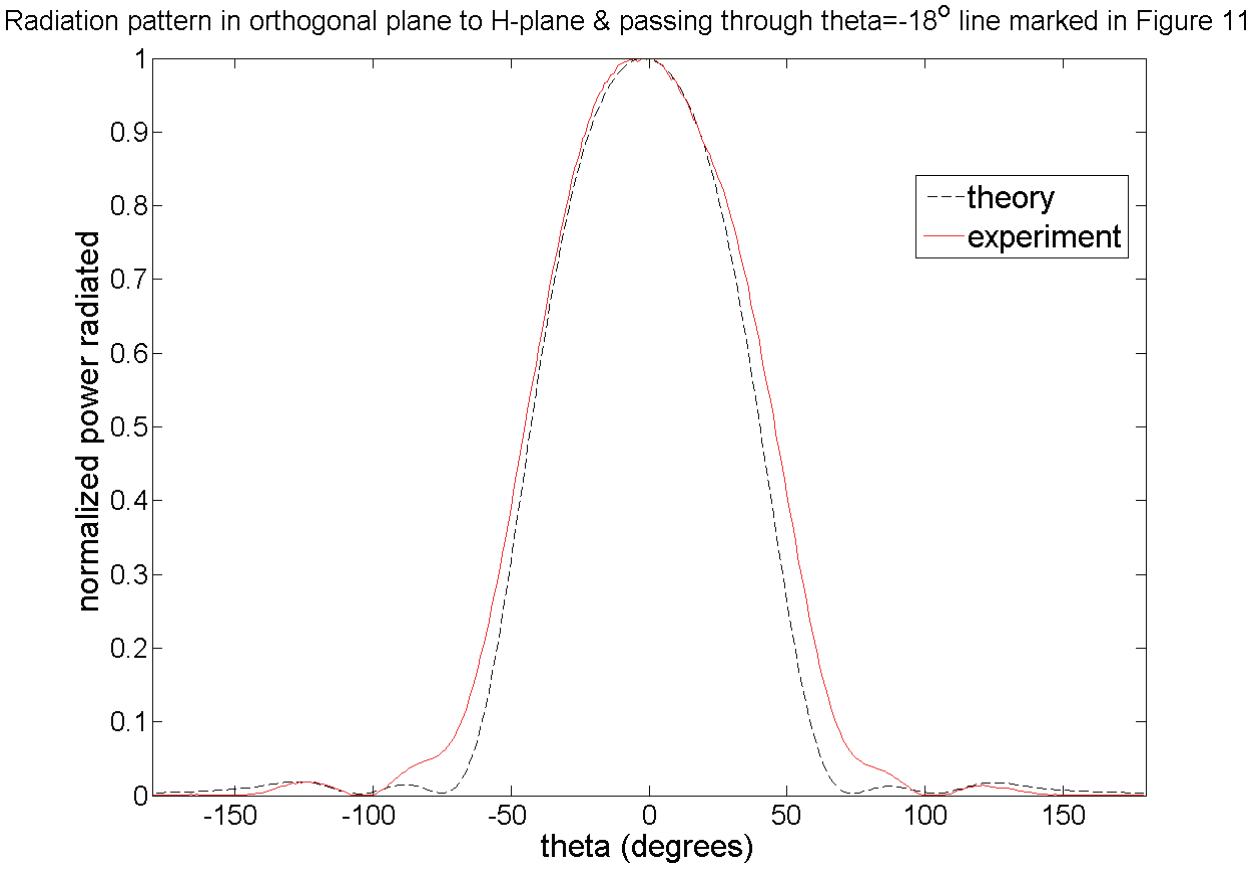

Fig. 12. X-band slot array's radiation pattern in the plane cut orthogonal to the H-plane and passing through the θ = -18° line shown in Fig. 11.

REFERENCES

[1] N. R. Devarapalli; **Rectangular waveguide narrow-wall longitudinal-aperture antenna arrays for high power applications**; Ph. D. thesis, University of New Mexico, Albuquerque, NM 87131, USA, August 2009.

[2] C. E. Baum; **Sidewall Waveguide Slot Antenna for High Power**; Sensor and Simulation Notes, Note 503. http://www.ece.unm.edu/summa/notes/SSN/Note503.pdf

[3] C. E. Baum; **High Power Scanning Waveguide Array**; Sensor and Simulation Notes, Note 459. http://www.ece.unm.edu/summa/notes/SSN/Note459.pdf

[4] D. M. Pozar; **Microwave Engineering**; John Wiley & Sons, New York, 2005.